February 2006

Fabricating Three-Dimensional Polymeric Photonic Structures by Multi-Beam Interference Lithography

Jun Hyuk Moon
University of Pennsylvania

Jamie Ford
University of Pennsylvania

Shu Yang
University of Pennsylvania, shuyang@seas.upenn.edu

Postprint version. "This is a preprint of an article published in *Polymers for Advanced Technologies*, Volume 17, Issue 2, 2006, pages 83-93."
Publisher URL: http://dx.doi.org/10.1002/pat.663

Fabricating Three-Dimensional Polymeric Photonic Structures by Multi-Beam Interference Lithography

Abstract

The fabrication of true three-dimensional (3D) microstructures both rapidly and economically over a large area with negligible defects is attractive for a wide range of applications. In particular, multi-beam interference lithography is one of the promising techniques that can mass-produce polymeric 3D photonic crystals defect-free over a large area. This review discusses the relationship between beam geometry and the symmetry of the interference patterns, the lithographic process, and various types of photoresist systems, including thick films of negative-tone and positive-tone photoresists, organic-inorganic hybrids, hydrogels, and holographic polymer-dispersed liquid crystals.

Keywords

photoresists, interference lithography, microstructures, photochemistry, fabrication

Comments

Postprint version. “This is a preprint of an article published in *Polymers for Advanced Technologies*, Volume 17, Issue 2, 2006, pages 83-93.”
Publisher URL: http://dx.doi.org/10.1002/pat.663

Fabricating Three-dimensional Polymeric Photonic Structures By Multi-Beam Interference Lithography

Jun Hyuk Moon, Jamie Ford, and Shu Yang[1]

Department of Materials Science and Engineering, University of Pennsylvania, 3231 Walnut Street, Philadelphia, PA 19104, USA

[1] *Correspondence to*: S. Yang, Department of Materials Science and Engineering, University of Pennsylvania, 3231 Walnut Street, Philadelphia, PA 19104, USA.

Email: shuyang@seas.upenn.edu

Abstract

The fabrication of true three-dimensional (3D) microstructures both rapidly and economically over a large area with negligible defects is attractive for a wide range of applications. In particular, multi-beam interference lithography is one of the promising techniques that can mass-produce polymeric 3D photonic crystals defect-free over a large area. This review discusses the relationship between beam geometry and the symmetry of the interference patterns, the lithographic process, and various types of photoresist systems, including thick films of negative-tone and positive-tone photoresists, organic-inorganic hybrids, hydrogels, and holographic polymer-dispersed liquid crystals.

Key words: polymers, photoresists, interference lithography, microstructures, photochemistry

INTRODUCTION

A photonic crystal is a regularly structured material with a periodic modulation in refractive index, or dielectric constant, on a length scale comparable to the wavelength of the incident light. Interference of the light waves scattered from the dielectric lattice (*i.e.* Bragg scattering) leads to stop bands or photonic band gaps (PBG), which are analogous to the electronic energy bandgaps in a semiconductor.[1,2] The bandwidth and the frequency of the PBG will be determined by the refractive index contrast, the lattice symmetry, and the volume fraction of high-index materials. A photonic crystal that has a complete PBG is highly desired since it acts like an optical trap to reflect incident light from any direction. Thus, controlled defects can be engineered into the 3D structures to confine or guide photons of specific wavelengths. Photonic crystals potentially offer revolutionary advances in numerous applications, including ultra-high-bandwidth integrated optical circuits, lasers, sensing, spectroscopy, and pulse shaping.

Although major progress has been made in the fabrication of two-dimensional (2D) photonic crystals, significant challenges remain for the fabrication of true three-dimensional (3D) photonic crystals. A promising 3D fabrication technique should be able to:

1) produce sub-micron periodicity for near-IR telecommunication wavelength (λ of 1.33 and 1.55 μm)
2) access a large number of structures with tailored shapes, functionalities, and sizes
3) allow mass-production in a large area
4) provide fine control of defects
5) create structures with a large index contrast (e.g. $n \geq 2$ for diamond symmetry) for a wide bandgap.

Many 3D fabrication approaches and materials have been investigated. For the large-scale fabrication of submicron features, it mainly relies on the optical projection lithography developed for silicon IC manufacturing. This method is inherently limited to 2D patterning and requires laborious layer-by-layer photolithography and etching processes to generate the continuous 3D structures.[3-6] A set of different chrome masks is required to form each of the different layer s using conventional projection lithography.[7] The masks for the lithographic pr ocesses are expensive and contribute a significant portion to the total cost for t he multi-level fabrication process of microstructures. Furthermore, precise opti

cal systems with vertical and horizontal steppers are required for repositioning and registration. The fabrication is thus practically limited to a few layers.

Self-assembly approaches, such as crystallization of colloidal particles[8,9], microphase separation of block copolymers[10], and soft-lithography[11] are simple and inexpensive, yet random defects, such as missing particles, uncontrolled orientation, phase mixing, and dislocations, are inevitable over a large area. The lattice symmetries resulted from colloidal assembly are rather limited, typically hexagonal close-packed (hcp) and face-centered-cubic (fcc) structures. Other 3D microfabrication techniques, such as three-axis micropositioner assisted deposition of polymer melts and solutions (e.g. rapid prototyping[12,13], pressure assisted microsyringe deposition[14], focused-ion-beam etching[15], and direct-write assembly[16,17], etc.), layer-by-layer stacking through soft lithography[18], glancing angle deposition (GLAD)[19], and multi-photon absorption at near-IR [20-26] have been studied to create arbitrary microstructures. However, *multiple processing steps* are typically involved. .

Recently, multi-beam interference lithography has gained much attention as an attractive candidate to fabricate polymeric 3D photonic crystals. It is based on the optical patterning of photopolymers and use a *single exposure* (a few nanoseconds to seconds). It has been demonstrated for various applications, including photonic

crystals[27-34], microlens arrays[35], information storage[36], and optical communication.[37,38] The interference lithography allows for precise control over the size and shape of the resulting structures, and can assess a much wider range of lattices than colloidal assembly through the proper arrangement of laser beams. However, the number of accessible lattice symmetries and lattice size could be limited by the index mismatching between the polymer and substrate, and the available space to arrange multiple beams. Furthermore, it is not straightforward to introduce defects with precise registration by multi-beam interference lithography itself alone. Possible solutions to address the symmetry include the use of phase shift mask and translational stages; while the use of index matching fluid and photoresists, and multiple exposures will allow better control of lattice size and its scalability. Since it is compatible with multi-photon lithography, which relies on similar photochemistry to pattern arbitrary structures in polymers, many researchers are exploring the possibilities to integrate multi-beam interference lithography and 2-photon lithography. It will enable fast production of 3D structures with controlled, functional elements (e.g. cavity defects and waveguides) *in situ* through sequential exposures to multi-photon and interference beams, or *vice versa.*

Multi-beam interference lithography

When two or more optical waves are present simultaneously in the same region of space, the waves interfere and generate a periodic spatial modulation of light[39]. Interference among any N (≤4) collimated, coherent laser beams produces an intensity grating with (N-1) dimensional periodicity if the difference between the wave vectors is non-coplanar. As shown in Fig 1, two interfering beams form a 1D fringe pattern (Fig. 1a) and three crossed beams form a 2D hexagonal pattern (Fig. 1b).

The intensity distribution of the interference field can be described by a Fourier superposition:

$$I = \sum_{i=1}^{N} |\mathbf{E}_i|^2 + \sum_{i \neq j}^{N} \mathbf{E}_i^* \cdot \mathbf{E}_j \exp[i\{(\mathbf{k}_j - \mathbf{k}_i) \cdot \mathbf{r} + (\varphi_j - \varphi_i)\}] \qquad (1)$$

where $\mathbf{r}$ is the position vector, $\mathbf{E}_i$, $\mathbf{k}_i$ and φ_i are the complex amplitude, wave vector, and phase of the *i*th beam, respectively. The complex amplitude vector of the *i*th wave can be written as

$$\mathbf{E}_i = E_i \exp(i\mathbf{k}_i \cdot \mathbf{r} + \varphi_j) e_i \qquad (2)$$

where E_i, and e_i are the *i*th wave's real amplitude and polarization vector, respectively. The difference between two of the wave vectors ($\mathbf{k}_i - \mathbf{k}_j$), where $i, j = 1,2, \ldots, N$ and $i<j$, determines the spatial periodicity, or translational symmetry of the interference pattern.[40-43] The contrast of the interference pattern is controlled by the real amplitude,

polarization and phase of each beam. The combination of these parameters determines the overall symmetry and contrast of the resulting lattice.[32,34,44,45]

Multi-beam interference previously has been used to write hologram gratings, to create optical traps for laser-cooled atoms[46], and to pattern optical tweezer arrays.[47-49] Recently, it has been integrated with lithography to produce periodic structures with sub-micron resolution in photoresists.[27-31,34] The photochemistry and lithographic processes involved in multi-beam interference are similar to those in conventional lithography except that photomasks are not required, and the substrate is typically transparent since all of the beams are not necessarily launched from the same side of the substrate.

Because the multiple beams must be coherent to produce an interference pattern, one laser beam from a visible (e.g. Ar-ion, frequency-doubled Nd:YAG, and Nd:YVO_4) or UV (e.g. frequency-tripled Nd:YAG and He-Cd) laser is typically divided into multiple beams using beam-splitters. The split beams are then recombined by mirrors to obtain the desired geometry. The polarization, intensity and phase of the beams are controlled by half-wave plates, polarizers, and quarter-wave plates, respectively. An experimental setup to perform 4-beam interference lithography is illustrated in Fig. 2. The combined beams are then focused on a relatively thick

photoresist film (up to100 μm) for a few nanoseconds to seconds, depending on the resist sensitivity and laser power from a pulsed or a continuous wave (cw) laser. In a negative-tone photoresist, the exposed regions are crosslinked when the intensity of the interference pattern exceeds the lithographic threshold of the photoresists. The unexposed regions are washed away by a developer (typically an organic solvent), resulting in a porous film. The threshold intensity is determined by the sensitivity of the photoresist and post-exposure processing (e.g., baking time and temperature, choice of developers and developing time), as well as the contrast of the interference pattern. In positive-tone photoresists, the exposed regions are removed by the developer (typically an aqueous base), while the unexposed or weakly exposed regions remain. Currently, most of the thick photoresists are negative-tone. Positive-tone resists may have higher resolution and better contrast because the resists are typically chemically amplified and there is a large polarity change in the aqueous base developer before and after the lithography.

Formation of two-dimensional (2D) microstructures

2D interference patterns can be obtained using different interference techniques, including interference by three focused beams[50], multiple diffraction

grating masks[29,51,52], and double exposures of a two-beam interference pattern.[53,54]

In the first case, the configuration of three focused beams determines the translational symmetry of the 2D pattern. Here we briefly introduce the practical setup for several 2D lattices. As shown in Fig. 3a and 3b, three beams are set to have the same polar angles to the z-axis of an arbitrary xyz-coordinate space, and are described as $\mathbf{k}_i = 2\pi/\lambda(\cos\phi_i \sin\theta, \sin\phi_i \sin\theta, \cos\theta)$, for *i*=1,2,3. The difference between two wave vectors lies within the xy-plane, producing a 2D interference pattern with basis vectors of $\mathbf{b}_1 = (\mathbf{k}_1 - \mathbf{k}_2)$ and $\mathbf{b}_2 = (\mathbf{k}_2 - \mathbf{k}_3)$ in the reciprocal lattice (Fig. 3d). Subsequently, the lattice constants and the angle between basis vectors in real space can be expressed as $\mathbf{a}_1 = \frac{\lambda}{|\sin\theta(\cos\phi_1 - \cos\phi_2)|}$, $\mathbf{a}_2 = \frac{\lambda}{2|\sin\theta \sin\phi_2 \sin((\phi_1 + \phi_2)/2)|}$, and $\gamma = (\phi_1 + \phi_2)/2$, where λ is the wavelength of the laser (Fig. 3a). The experimental conditions for 2D square and tetragonal lattices are shown in Table 2.[33] For the square lattice, Eq (1). becomes

$$I = \sum_i^3 |\mathbf{E}_i|^2 + \mathbf{E}_1 \cdot \mathbf{E}_2 \cos[2\pi x/\mathrm{a}] + \mathbf{E}_2 \cdot \mathbf{E}_3 \cos[2\pi y/\mathrm{a}] \qquad (3)$$

The symmetry of the "atoms" in the "basis" is dependent on the polarization of the beams as shown in Fig. 4 by changing the ratios of $(\mathbf{E}_1 \cdot \mathbf{E}_2)/(\mathbf{E}_2 \cdot \mathbf{E}_3)$.

When a grating mask is used to pattern a photoresist, the incident beam is diffracted by three or four diffraction gratings aligned at an angle.[52,55] The first-order

diffracted beams interfere and produce the pattern. Compared to the three-beam setup, this method is more stable due to the use of a single monolithic diffracting object. Since the interference pattern depends on the period of the gratings and the angle between gratings, different grating masks will be required to vary the size of the pattern.

In addition to the two techniques mentioned above, which are based on a single exposure of three beams, 2D patterns can also be obtained through multiple exposures with a two-beam interference pattern.[53,56,57] In practice, it is much more convenient to arrange two beams with different geometries to access a wide range of lattices with variable unit sizes and large contrast. For example, both square and tetragonal 2D lattices can be obtained by simply rotating the sample stage with precise control over the in-plane rotation of the substrate.

Formation of three-dimensional (3D) microstructures

3D microstructures have been created using four-beam interference[27,30,31], diffraction grating masks[28], multiple exposure techniques[34,58], and phase masks on a controlled stage.[59] 3D lattices that possess large photonic band gaps, including simple cubic, face-centered cubic (f.c.c), diamond, body-centered cubic (b.c.c), and gyroid lattices have

been demonstrated both theoretically and experimentally,[32,34,60-62] thus, will be the focus of this review.

It has been predicted that the translational symmetries associated with all 14 Bravais lattices can be accessible through multi-beam interference lithography[43], however, little attention has been paid to the effect of the beam polarization on the overall symmetry until recently. As shown in the formation of 2D patterns, the symmetry of the "atoms" in the "basis" will be affected by the beam polarization vectors (Fig. 4). When the polarizations are taken into account, the overall symmetry of the interference pattern may not respect all the required site symmetries of the particular Bravais lattice, or correspond to any one of the space groups of the originally specified Bravais lattice. Clearly, there is a need to establish a better understanding of the relationship between the resulting symmetries and the beam parameters.

A level-set approach has been proposed to equate terms of the intensity equation to a representative level surface of the desired space group.[45] This method was previously used to describe minimal surfaces in microphase-separated morphologies, such as those typically found in block copolymer systems.[63] In this approach the complete symmetry of the 3D lattice is defined by its structure factors. The level surfaces are functions that are of the form F: $\mathbf{R}^3 \rightarrow \mathbf{R}$ of points $\{x, y, z\} \in \mathbf{R}^3$

that satisfy the equation $F(x, y, z) = t$, where t is a constant. When $F(x,y,z)=0$, it defines a boundary between positive F and negative F. Specifically, a candidate structure can be modeled using a 3D surface given by $F(x,y,z)-t=0$. By varying the value of the constant t, which is achieved experimentally by adjusting the threshold value of the photoresist[30,64], we can access a family of surfaces with different volume fractions to tune the photonic band structure. When equating terms of the intensity equation to a level surface, we can calculate the beam parameters (wave vectors, polarizations, intensity, etc.) to construct a desired 3D lattice. For example, the three-termed simple-cubic, diamond-like (fcc translational symmetry) and gyroid-like (bcc translational symmetry) structures have been calculated using the level-set approach (see Table 3).[34] The equations describing these structures are given by

$$F(x, y, z) = \sin(x) + \sin(y) + \sin(z) + t \quad (4)$$

for a simple cubic surface,

$$F(x, y, z) = \sin(-x+y+z) + \sin(x-y+z) + \sin(x+y-z) + t \quad (5)$$

for a diamond-like structure, and

$$F(x, y, z) = \sin(y+z) + \sin(y-z) + \sin(-x+z) + t \quad (6)$$

for a gyroid structure, respectively. The plots of the corresponding isointensity surfaces are shown in Fig. 5.

PHOTOSENSITIVE MATERIALS AND THEIR APPLICATIONS

Negative-tone photoresists

To fabricate 3D polymeric photonic crystals, a thick photoresist film is usually required for a multi-layer unit cell. Negative-tone pohotoresists, such as SU-8, are commonly used for thick films (thickness up to 2 mm with an aspect ratio ≥ 20). SU-8 has high solubility in many organic solvents, which enables the preparation of thick films and it is highly transparent in the near-UV and visible region. Commercially available SU-8 photoresists (Microchem Inc.) consist of EPON SU-8, a derivative of bisphenol-A-novolac resin with an average of eight epoxy groups, triaryl sulphonium salts as photoacid generators (PAG)[65] (see Scheme 1), and γ-butyrolactone (GBL) or cyclopentanone (CP) as a solvent. The solution is spun onto a cover glass and baked on a hotplate at 95°C to evaporate the solvent. During UV exposure, the triaryal sulfonium salts release photoacids in localized regions. The subsequent post-exposure bake above the glass transition temperature of SU8 (50^{o}C) accelerates acid diffusion and induces cationic polymerization of the epoxy groups in SU-8.[66-68] The unexposed film is removed by propylene glycol methyl ether acetate (PGMEA), followed by supercritical CO_2 drying to prevent pattern collapse caused by capillary force during

drying. The low surface tension of supercritical CO_2 is especially advantageous in removing solvents from films with high porosity and high aspect ratio features. The resulting SU-8 film is highly crosslinked and exhibits excellent thermal (Tg > 200°C) and high mechanical strength (Young's modulus, E > 4.0 GPa).

The relatively high glass transition temperature of SU-8 plays an important role in minimizing acid diffusion before the post-exposure bake. A high glass transition temperature has been one of the key resist design criteria to achieve submicron resolution in deep UV lithography of chemically amplified photoresists. It becomes even more important in interference lithography since polymerization during exposure is not desired; this would disturb the original interference pattern due to the change in refractive index of the crosslinked film. When the film is exposed at room temperature and then baked at 95°C, the exposure and crosslinking stages are separated.

Although SU-8 resin is quite transparent in the near-UV region, it is more appealing to perform interference lithography using visible light. Not only is the visible continue wave (cw) laser more readily accessible in the lab than the UV pulsed laser, but a longer wavelength affords a larger lattice period. Furthermore, the SU-8 photoresists is highly transparent in the visible region, therefore interference of visible light (i) is applicable to a wide range of photosensitive materials, and (ii) provides a

more even exposure throughout the thick films.

Since most photoacid generators do not response to visible light, the resists are formulated based on visible laser-sensitized cationic polymerization of epoxides.[69,70] This initiating system typically includes a photosensitizer, which absorbs the visible light and transfers an electron to an onium salt via the formation of a charge transfer complex to generate the acids (see Scheme 2). Typically diaryliodionium salts are chosen as photoacid generators instead of triarylsulfonium salts due to the low reduction potential of iodionium salts for energy transfer. The photoacids initiate ring-opening reactions of the epoxy groups and the acids are regenerated in the subsequent steps.[71,72] The polymerization is thus chemically amplified, resulting in a highly crosslinked film. Several visible photosensitizer/PAG systems for SU-8 photoresists have been developed, including xanthene dyes, 2,4,5,7-tetraiodo-6-hydroxy-3-fluorone (H-Nu 535 from Spectra Group Ltd.) and diaryliodionium hexafluoroantimonate (SR1012 from Sartomer)[30], 5, 7-diiodo-3-butoxy-6-fluorone (H-Nu 470 from Spectra Group Ltd.) and octoxyphenylphenyl-iodonium hexafluoroantimonate (Uvacure 1600 from UCB) [50, 64], and H-Nu 470 and phenyl-p-octyloxyphenyl-iodoniumhexafluoroantimonate (OPPI from Spectra Group Ltd.).[59] A single photoinitiation system, (η^6-naphthalene)(η^5-cyclopentadienyl)-iron(II)

hexafluorophosphate (Irgacure 261 from Ciba Specialty Chemicals), which has absorption in visible light and generates Lewis acids upon exposure, has also been demonstrated.[31, 35]

To produce a clearly defined, completely open porous 3D pattern, a high pattern contrast is necessary. In multi-beam interference, the partially non-parallel polarization of three or four non-coplanar laser beams produces a non-zero background intensity ($I_0 > 0$) and, therefore, a non-zero background of generated acids ($C_0 > 0$) (Figure 6). This results in the formation of shallow patterns without fully opened pores throughout the film (Figure 7a). Although the non-zero background of the interference intensity could be minimized by fine-tuning the beam polarization, it may alter the overall symmetry of the final lattice. Instead, a chemical approach that controls the acid generation will be preferred.

In conventional photolithography, control of acid diffusion plays a pivotal role to improve shelf life, resolution, and resist contrast.[73] Base additives have been used as acid scavengers to (i) extend shelf life for low activation systems, such as ketal and acetal protected poly(hydroxystyrene), (ii) improve contamination resistance for high activation resist systems, such as *t*-BOC and *t*-butyl ester resins, and (iii) reduce line width slimming and post-exposure bake sensitivity. More importantly, base additives

can be used to minimize acid diffusion and enhance chemical contrast during the exposure and bake processes, hence improving the resolution. With the addition of an appropriate amount of triethyl amine (TEA), which partially neutralizes the local photoacids generated by I_0 during exposure, we have successfully eliminated the homogeneous crosslinked background, resulting in a completely open structure throughout the film (see Fig 7b and 7c).

An alternative approach is to optimize the loading of the photosensitizers.[64] Fig. 8 shows the sensitivity curve of the SU-8 photoresist as a function of 2-beam interference exposure dose. Here, the sensitivity represents the normalized pattern contrast defined as the feature size (*d*) scaled by the feature distance (*p*). The contrast of a negative-photoresist pattern is related to the rates of both crosslinking and dissolution by the developer solution. A steeper change in crosslinking with dose energy creates a higher contrast pattern. Therefore, the slopes of the sensitivity curves in Fig. 8 indicate that the highest contrast pattern is obtained from the film loaded with 0.5 wt% H-Nu470 photosensitizer.[64]

Positive-tone Photoresists.

Although various types of 3D photonic structures have been fabricated using

multi-beam interference lithography, none has shown complete PBG properties due to the low refractive index of polymers (e. g. SU-8, n= 1.59). To increase the refractive index contrast, polymeric photonic crystals can be used as sacrificial templates for infiltration of a higher index inorganic material, followed by the removal of polymers, resulting in inverse 3D structures. Currently most of the 3D polymer microstructures are created in negative-tone photoresists, which form highly crosslinked 3D networks that are difficult to remove by solvent and heat below 400^{o}C. It will be advantageous to pattern 3D structures in positive-tone resists that can be easily dissolved in an organic solvent after infiltration. Preliminary results have been obtained using a commercially available positive-tone resist, AZ5214 (Clariant International Ltd.). AZ5214 is a two-component resist system, a novolac resin as matrix and a diazonaphthoquinone as photoactive component or sensitizer. Upon exposure, the base-insoluble diazonaphthoquinone undergoes photolysis and Wolff rearrangement to form a ketene (see Scheme 3).[74] In the presence of trace water, the ketene forms a base-soluble indenecarboxylic acid and generates a positive-tone feature. The unexposed regions can be removed with acetone. As seen in Fig. 9, a 2D hexagonal pattern was generated from three-beam interference lithography using the same optics setup reported in the literature for the fabrication of biomimetic microlens arrays in the

negative-tone resist, SU-8.[35] It seems to suggest that positive-tone resists give better contrast and sharper corners than negative-tone resists.

Organic-inorganic hybrids

As discussed above, a 3D polymer structure can be infiltrated with a higher refractive index material into the pores to obtain an inverse 3D photonic crystal. For example, an anatase titania replica can be obtained from fcc-like SU-8 as shown in Fig. 10. The titania was deposited from titanium tetrachloride ($TiCl_4$) in a batch reactor under atmospheric pressure at room temperature, followed by calcination at 500 ˚C to remove the polymer template.

Back-filling and calcination processes often suffer from volume shrinkage that causes fracture and loss of long-range order, as well as incomplete filling. An alternative approach is to directly pattern from an organic-inorganic hybrid photoresist. For example, organosilicates can be obtained from the sol-gel reaction of 3-methacryloxypropyl trimethoxysilane with water and an acid catalyst.[75] The addition of transition metal alkoxide precursors, such as zirconium propoxide and titanium propoxide, to methacrylic acid (MA) produces photocrosslinkable organic-inorganic composites. Depending on the transition metal content, the refractive index of the

hybrid can be increased to 2.0. Other titanium-containing photoresists have been synthesized from the mixture of titanium ethoxide (TE), methacrylic acid and ethylene glycol dimethacrylate (EGDMA).[52] The TE and MA produce the titania-acrylate composites while EGDMA acts as a crosslinker.

Hydrogels

Hydrogels have been widely used as responsive materials because they exhibit large volume and shape changes in response to external stimuli, such as pH and temperature. Photosensitive hydrogels have been used for microfluidic switches and actuators[76], tunable photonic materials[77], and controlled release materials.[78] Most existing hydrogel patterning approaches rely on the radical polymerization of liquid monomers, resulting in inhomogeneity of radical formation and the lack of control over radical diffusion, which limits the resolution of these systems to about 5μm. We have recently developed a photosensitive hydrogel precursor, poly(2-hydroxyethyl methacrylate-*co*-methyl methacrylate) (HEMA-*co*-MMA), which has a high Tg (>100^{o}C), and the hydroxyl groups of HEMA can be crosslinked by photoacid generators (PAG) and external crosslinkers, tetramethoxymethyl glycouluril (TMMGU). It has been applied to three-beam interference lithography to synthesize a soft, biomimetic microlens arrays

in a single exposure step for a few seconds. Thus obtained soft lens arrays have low shrinkage in the lattice size compared to that of the rigid ones from epoxy (SU8) with much improved resolution (minimum feature size up to ~600 nm) (see Fig. 11).[79] The hydrogel lenses are highly deformable in solvent due to their soft nature.

Since hydroxyl groups are readily available in biocompatible polymers, and can be coupled with a variety of functional groups though copolymerization, we believe the crosslinking mechanism depicted here might shed light on fabricating a variety of 3D hydrogel structures with tailored architectures, tunability and functionalities.

Holographic polymer-dispersed liquid crystals (H-PDLC)

Following the realization of 3D photonic structures, it will be interesting to incorporate active materials that will respond to physical and chemical stimuli for tunable electro-optical devices, for example, using responsive hydrogels as the matrix material. Another approach is to embed liquid crystals into the interstitial space of close-packed colloidal crystals.[80-82] Liquid crystals exhibit large optical anisotropy, and their refractive index can be tuned by electrical fields or temperatures to shift the stop-bands. However, sedimentation of colloidal particles could take hours to days,

and require multiple steps, including water evaporation, thermal annealing and back filling with liquid crystals. In comparison, in holographic polymer-dispersed liquid crystals (H-PDLCs), liquid crystals spontaneously phase-separate from the polymers to the regions of minimum intensity during holographic patterning, while multi-beam interference could offer a wide variety of crystal symmetries with size approaching sub-100 nm range. Similar to conventional PDLCs[83], a photosensitive syrup consists of multi-functional photocrosslinkable monomers, such as tri-, penta- and hexa-functional urethane or acrylate oligomers, nematic liquid crystals, a visible photosensitizer, and radical initiators/co-monomers. Upon exposure to the interference of a visible light, liquid crystals are trapped in nanometer- to micron-sized droplets within a polymer matrix due to the rapid polymerization, resulting in a periodic pattern of polymer-rich and liquid crystal-rich regions. In the absence of an electrical field, H-PDLCs are highly scattering due to the index mismatch between polymers and unaligned liquid crystals. As the applied voltage increases, the LC directors reorient and yield a minimum index contrast between the polymers and LCs, therefore, lowering the diffraction efficiency.

1D anisotropic reflection gratings[84] and polarization gratings[85] have been obtained using two-beam interference. 2D and 3D tunable H-PDLCs, including

transverse square (Fig. 12a-c)[86], fcc (Fig. 12d-f)[87], diamond-like fcc[88], and orthorhombic P lattices(Fig. 12g-i)[89] have been demonstrated using three-beam, four-beam, and six-beam interference, respectively (see Fig. 12).

SUMMARY

Multi-beam interference lithography reviewed here is a promising method to photopattern periodic one-, two-, and three-dimensional polymeric photonic structures with sub-micron periodicity defect-free in a large area. The symmetry and size of the lattice can be controlled by varying the intensity, geometry, polarization and phase of the beams. The versatility of this technique has been demonstrated in various photoresist platforms, including UV and visible sensitive resists, negative-tone and positive-tone resists, hydrogels, organic-inorganic hybrids, and holographic polymer-dispersed liquid crystals. The ability to engineer 3D microporous materials using multi-beam interference may offer valuable insights to a wide range of potential applications including photonics, data storage, chemical sensors, nano- and microfludic networks, and tissue engineering.

ACKNOWLEDGMENT

The authors are grateful to the students, postdoctoral researchers, and other collaborators who are involved in the work described in the review. This work is supported by the Office of Naval Research (ONR) through the MURI program, Grant # E-21-6WG-G2, the Skirkanich Chair of Innovation (SY), and the Korea Research Foundation postdoc fellowship (JHM), Grant # KRF-2005-000-10299.

Table and Figure Captions:

Table 1. A comparison of different types of 3D microfabrication techniques.

Table 2. Experimental conditions for 2D square and tetragonal lattices and the resulting lattice constants of the interference patterns.[33]

Table 3. Beam parameters for four-beam interference of the three-termed simple cubic, diamond-like and gyroid-like surfaces, and the resulting lattice constants. *Source:* from ref.[34]

Scheme 1. The chemical structures of photoresist, SU-8, and photoacid generator, triaryl sulfonium salt.

Scheme 2. A general scheme for photosensitized cationic polymerization. *Source:* from ref.[30]

Scheme 3. Schematic illustration of the photochemistry of a diazonaphthoquinone-novolac resist. Adapted from ref.[74]

Figure 1. Optical images of (a) two- and (b) three-beam (*Source:* from ref.[44]) interference patterns.

Figure 2. Experimental setup for 4-beam interference lithography.

Figure 3. 2D lattices formed from three-beam interference: (a) beam geometry in perspective, (b) beam geometry within the XY-plane showing reciprocal wave vectors, (c) resulting lattice, and (d) associated reciprocal lattice. *Source:* from ref.[33]

Figure 4. The effect of beam polarization on a square interference pattern. The ratio of $\mathbf{E}_1 \cdot \mathbf{E}_2$ and $\mathbf{E}_2 \cdot \mathbf{E}_3$ is (a) 2, (b) 1, and (c) 0.5, respectively.

Figure 5. The isointensity surfaces of three-termed simple cubic, diamond-like, and gyroid-like structures. *Source:* from ref.[34]

Figure 6. Non-zero backgrounds (▨) of the light intensity and the resulting acid concentration generated in the interference pattern of non-orthogonally polarized beams. Source: from ref.[30]

Figure 7. Scanning electron micrographs (SEM) of micropatterned 3D polymer films. (a-c) Top view of the fcc-like structures formed in the absence (a) and in the presence (b) of TEA. (c) Cross-section of the fractured, continuously porous film shown in (b). The top surface is a (111) plane and the fractured surface is a (100) plane. The scale bar is 2 μm. *Source:* from ref.[30]

Figure 8. Sensitivity curve of visible SU-8 photoresists with different loadings of photosensitizers. *Source:* from ref.[64]

Figure 9. SEM image of micropatterned AZ 5214 polymer films by three-beam interference lithography.

Figure 10. A fcc-like SU-8 photoresist pattern (inset) and its anatase titania replica. Scale bar, 5 μm.

Figure 11. SEM of hydrogel microlens arrays formed from poly(2-hydroxyethylmethacrylate-*co*-methylmethylmethacrylate) by three-beam interference lithography. Scale bar, 5 μm. Source: from ref.[79]

Figure 12. Different types of 2D and 3D lattices from H-PDLCs. (a) Calculated isointensity surface, (b) arrangement of beams, and (c) SEM image of XZ-face of cylindrical cavities. *Source:* from ref.[86] (d) Calculated isointensity surface, (e) ideal propagation vectors within the film ($\theta \approx 63^{o}$), and (f) SEM image of polymer morphology of the fcc lattice in H-PDLC. *Source:* from ref.[87] (g) Calculated isointensity surface of YZ-plane, (h) laser beam geometry, and (i) SEM image of (100) plane after removal of the liquid crystals in orthorhombic P lattice. Scale bar, 250 nm. *Source:* from ref.[89]

Table 1. A comparison of different types of 3D microfabrication techniques.

Technique	Materials	Typical Dimensions (WxDxH)	Patterning Speed	Resolution	3D structures
Self-assembly[8,10]	monodispersed polymeric or inorganic particles, block copolymers	Continuous particle deposition: 100mmx100μmx10μm	seconds to days	10 nm	Periodic
Multi-beam interference lithography[27,30,33]	photosensitive polymer films (organic, hybrids)	Single and multiple exposures: 10mmx10mmx100μm	ns to seconds	300 nm	Periodic
Rapid protyping[12,13]	concentrated particle gels, colloidal gels, polymer solutions	Layer-by-layer deposition: 10mmx10mmx10mm	several mm/s	100 μm	Arbitrary
Direct-write assembly[16,17]	polyelectrolyte, concentrated colloidal gels, nanoparticle gels	Layer-by-layer writing: 10cmx10 cmx5 cm	250 μm/sec	< 1 μm	Arbitrary
Multi-photon absorption[20-22,26]	photosensitive monomeric liquids, polymer films, metal nanoparticles	Serial writing: 100μm x100μmx50μm	9 cm/s	120 nm	Arbitrary
GLAD[90,91]	semiconductors, metals, metal oxides, and fluorides	Rotate and step: 5cmx5cmx 8 μm	2-10Å/s	Pitch of 10's nm	chevrons, zig–zags, helical columns, superhelical

Table 2. Experimental conditions for 2D square and tetragonal lattices, and the resulting lattice constants of the interference patterns.[33]

Lattice	The angle against z-axis, ϕ_i	Lattice constant, $\mathbf{a}_i$
Square	$\phi_1 = \pi/4$, $\phi_2 = 3\pi/4$, $\phi_3 = -3\pi/4$	$\lvert\mathbf{a}_1\rvert = \lvert\mathbf{a}_2\rvert = 0.707\lambda/\sin\theta$
Tetragonal	$\phi_1 = 0$, $\phi_2 = 2\pi/3$, $\phi_3 = -2\pi/3$	$\lvert\mathbf{a}_1\rvert = \lvert\mathbf{a}_2\rvert = 0.667\lambda/\sin\theta$

Table 3. Beam parameters for four-beam interference of the three-termed simple cubic, diamond-like and gyroid-like surfaces, and the resulting lattice constants. *Source:* from ref.[34]

Lattice	Wave vectors	Polarization Vectors	Lattice constant
Simple cubic	$k_0 = \pi / a[111]$ $k_1 = \pi / a[\bar{1}11]$ $k_2 = \pi / a[1\bar{1}1]$ $k_3 = \pi / a[11\bar{1}]$	$E_{00} = 1.00[0.0, 0.707, -0.707]$ $E_{01} = 0.632[-0.5, 0.309, -0.809]$ $E_{02} = 0.874[-0.5, 0.309, -0.898]$ $E_{03} = 2.288[-0.309, 0.809, 0.5]$	$\sqrt{3}\lambda / 2$
Diamond-like	$k_0 = \pi / a[333]$ $k_1 = \pi / a[511]$ $k_2 = \pi / a[151]$ $k_3 = \pi / a[115]$	$E_{00} = 4.897[0.612, -0.774, 0.161]$ $E_{01} = 4.000[0.25, -0.905, -0.346]$ $E_{02} = 5.789[0.346, -0.25, 0.905]$ $E_{03} = 12.94[0.905, 0.346, -0.25]$	$3\sqrt{3}\lambda / 2$
Gyroid-like	$k_0 = \pi / a[333]$ $k_1 = \pi / a[511]$ $k_2 = \pi / a[151]$ $k_3 = \pi / a[115]$	$E_{00} = 5.657[0.707, -0.707, 0]$ $E_{01} = 6.164[0.162, 0.162, -0.973]$ $E_{02} = 6.164[0.162, 0.162, -0.973]$ $E_{03} = 12.693[0.680, 0.680, -0.272]$	$3\sqrt{3}\lambda / 2$

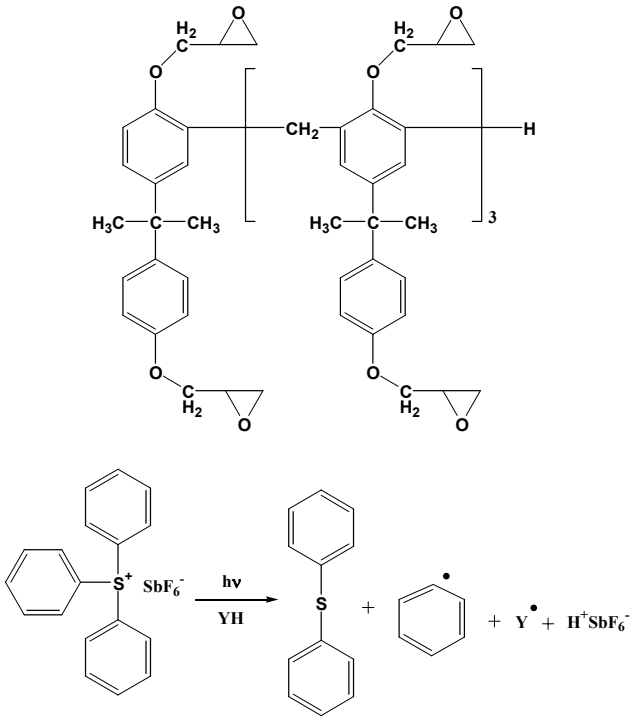

Scheme 1. The chemical structures of photoresist, SU-8, and photoacid generator, triaryl sulfonium salt.

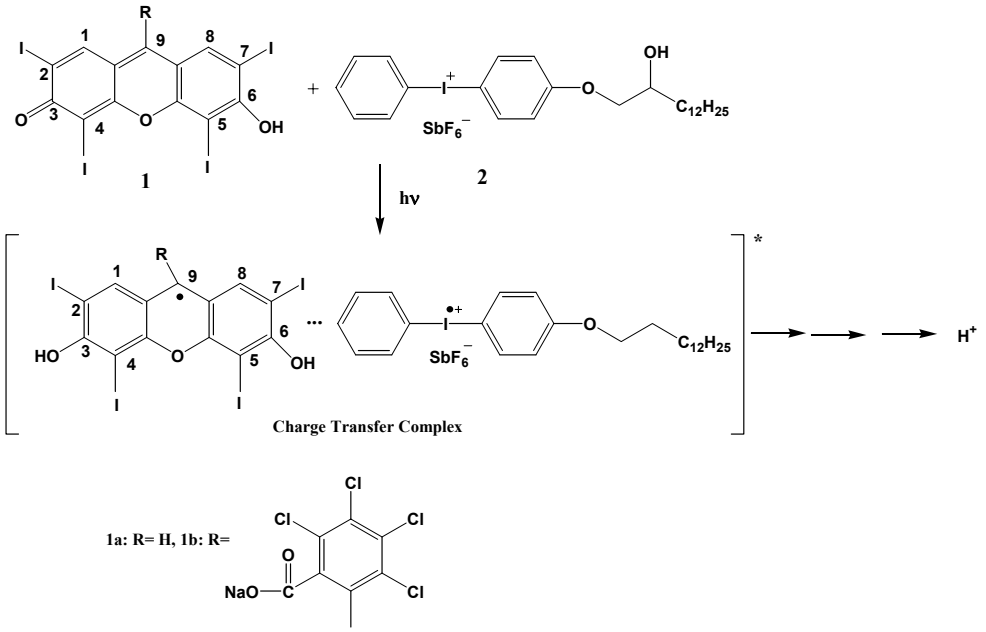

Scheme 2. A general scheme for photosensitized cationic polymerization. *Source:* from ref.[30]

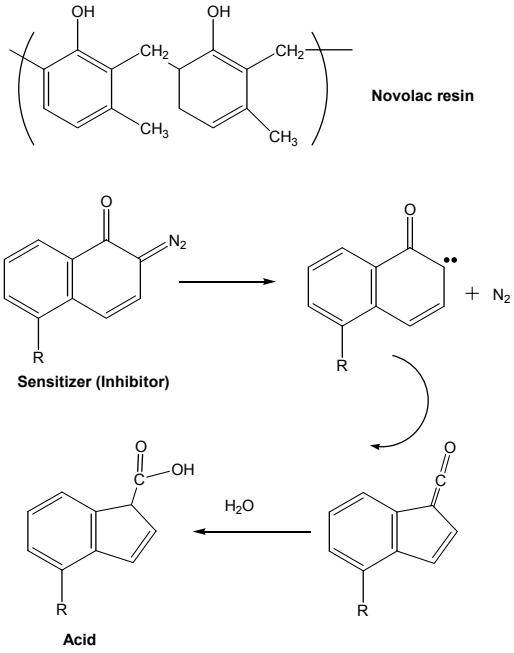

Scheme 5. Schematic illustration of the photochemistry of a diazonaphthoquinone-novolac resist. Adapted from ref.[74]

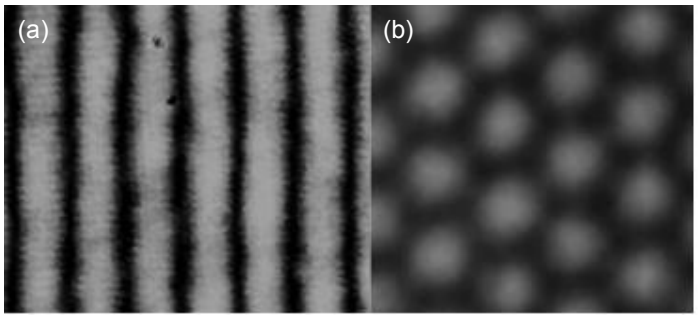

Figure 1. Optical images of (a) two- and (b) three-beam (*Source:* from ref.[44]) interference patterns.

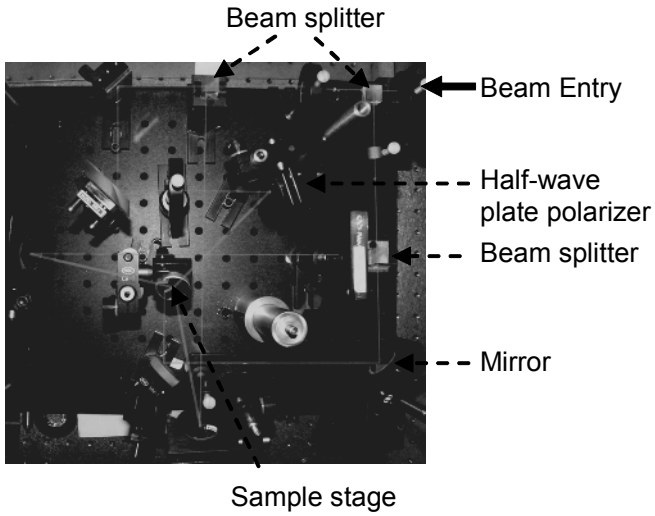

Figure 2. Experimental setup for 4-beam interference lithography.

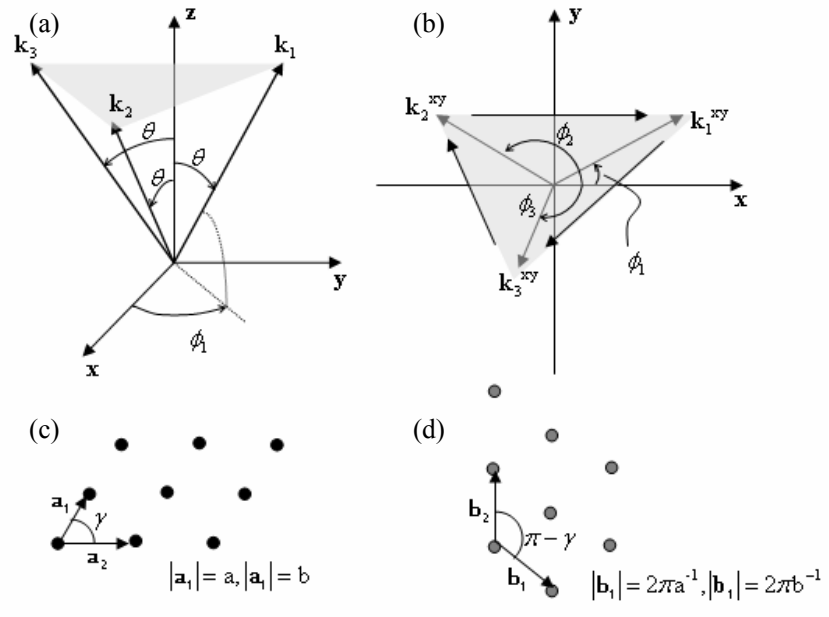

Figure 3. 2D lattices formed from three-beam interference: (a) beam geometry in perspective, (b) beam geometry within the XY-plane showing reciprocal wave vectors, (c) resulting lattice, and (d) associated reciprocal lattice. *Source:* from ref.[33]

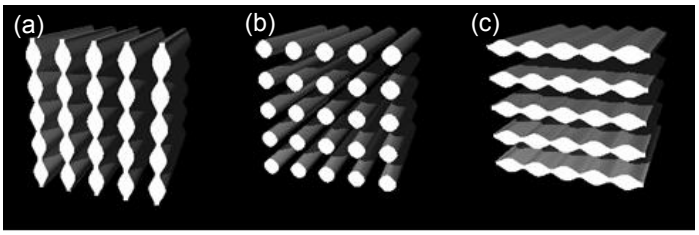

Figure 4. The effect of beam polarization on a square interference pattern. The ratio of $\mathbf{E}_1 \cdot \mathbf{E}_2$ and $\mathbf{E}_2 \cdot \mathbf{E}_3$ is (a) 2, (b) 1, and (c) 0.5, respectively.

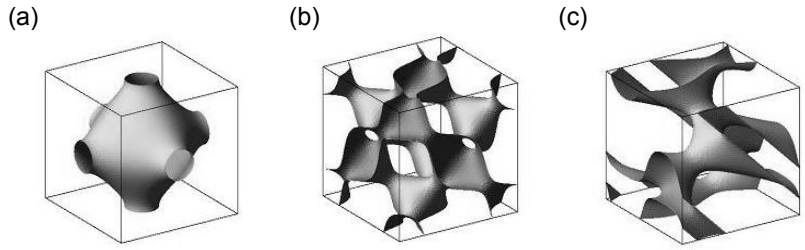

Figure 5. The isointensity surfaces of three-termed simple cubic, diamond-like, and gyroid-like structures. *Source:* from ref.[34]

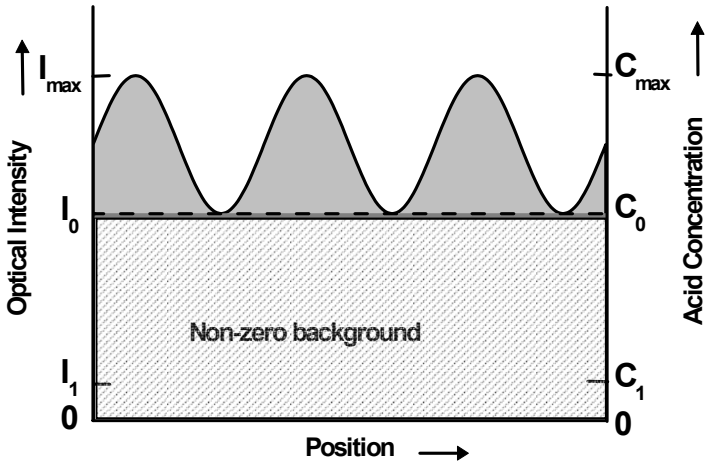

Figure 6. Non-zero backgrounds (▨) of the light intensity and the resulting acid concentration generated in the interference pattern of non-orthogonally polarized beams. Source: from ref.[30]

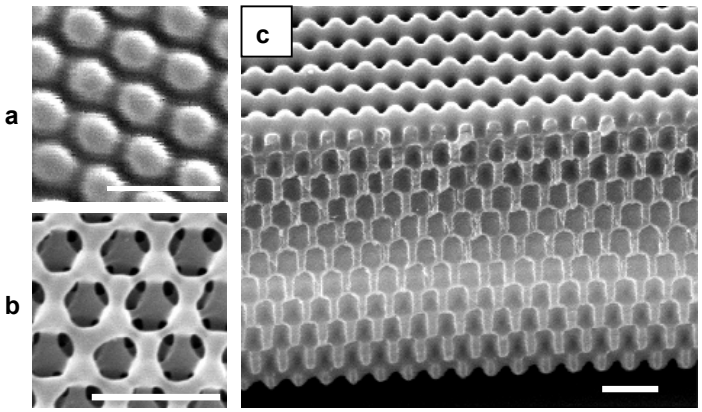

Figure 7. Scanning electron micrographs (SEM) of micropatterned 3D polymer films. (a-c) Top view of the fcc-like structures formed in the absence (a) and in the presence (b) of TEA. (c) Cross-section of the fractured, continuously porous film shown in (b). The top surface is a (111) plane and the fractured surface is (100) plane. The scale bar is 2 μm. *Source:* from ref. [30]

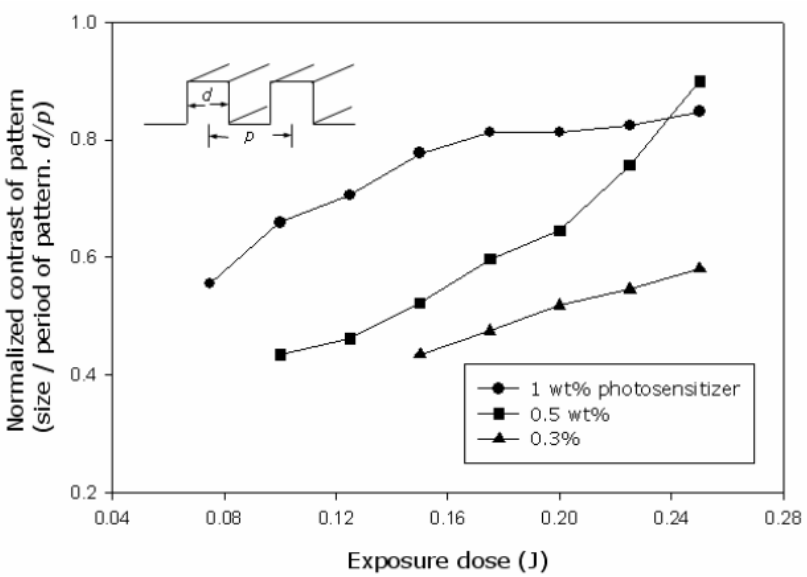

Figure 8. Sensitivity curve of the visible SU-8 photoresists with different loadings of photosensitizers. *Source:* from ref.[64]

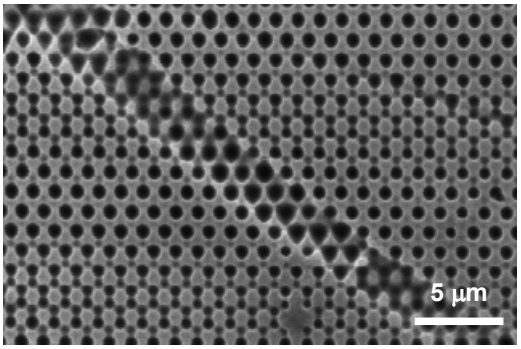

Figure 9. SEM image of micropatterned AZ 5214 polymer films from three-beam interference lithography.

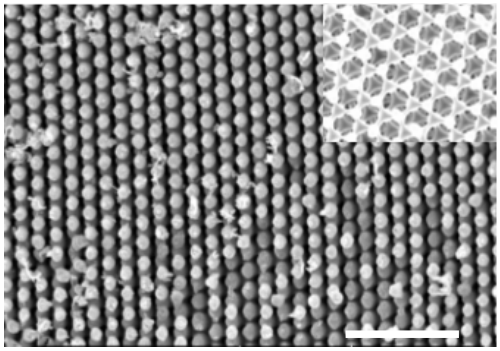

Figure 10. A fcc-like SU-8 photoresist pattern (inset) and its anatase titania replica. Scale bar, 5 μm.

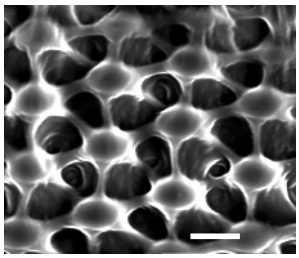

Figure 11. SEM of hydrogel microlens arrays formed from poly(2-hydroxyethylmethacrylate-*co*-methylmethylmethacrylate) by three-beam interference lithography. Scale bar, 5 μm. Source: from ref.[79]

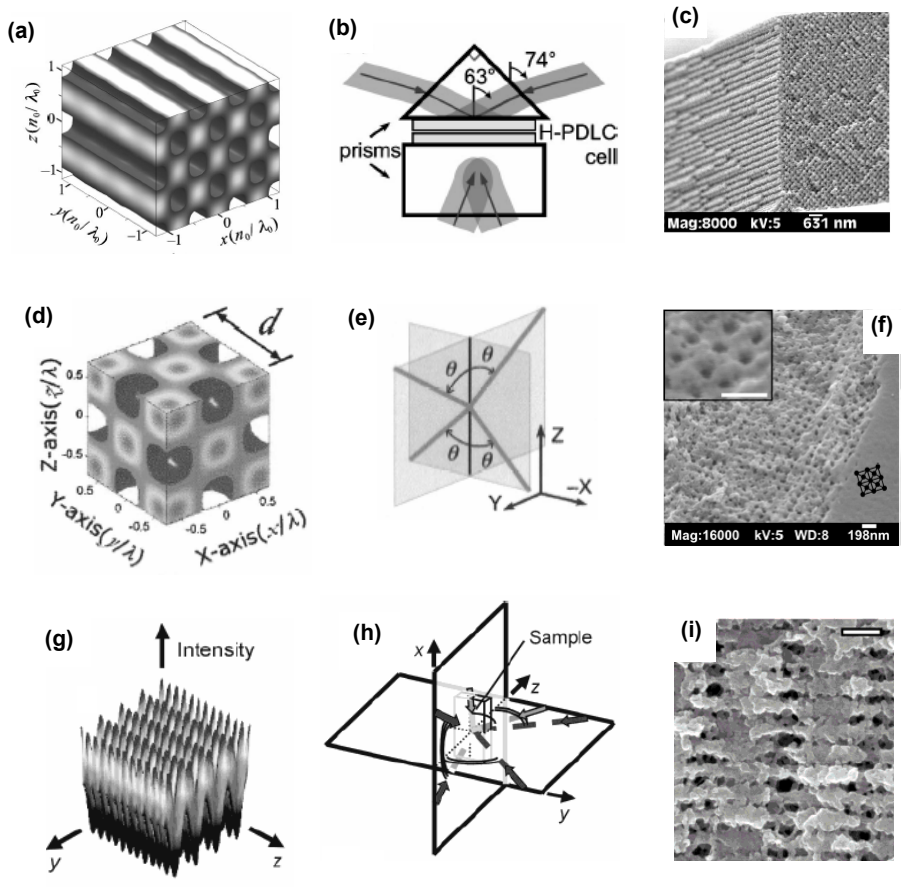

Figure 12. Different types of 2D and 3D lattices from H-PDLCs. (a) Calculated isointensity surface, (b) arrangement of beams, and (c) SEM image of XZ-face of cylindrical cavities. *Source:* from ref.[86] (d) Calculated isointensity surface, (e) ideal propagation vectors within the film ($\theta \approx 63^{o}$), and (f) SEM image of polymer morphology of the fcc lattice in H-PDLC. *Source:* from ref.[87] (g) Calculated isointensity surface of YZ-plane, (h) laser beam geometry, and (i) SEM image of (100) plane after removal of the liquid crystals in orthorhombic P lattice. Scale bar, 250 nm. *Source:* from ref.[89]

REFERENCES

1 Yablonovitch E, Gmitter TJ. *Phys. Rev. Lett.* 1989; **63**: 1950.

2 Joannopoulos JD, Meade RD, Winn JN. *Photonic Crystals*; 1995; Princeton University Press, Princeton, NJ.

3 Qi J, Crawford GP. *Displays* 2004; **25**: 177.

4 Aoki K, Miyazaki HT, Hirayama H, Inoshita K, Baba T, Sakoda K, Shinya NAoyagi Y. *Nature Mater.* 2003; **2**: 117.

5 Johnson SGJoannopoulos JD. *Appl. Phys. Lett.* 2000; **77**: 3490.

6 Lin SY, Fleming JG, Hetherington DL, Smith BK, Biswas R, Ho KM, Sigalas MM, Zubrzycki W, Kurtz SRBur J. *Nature* 1998; **394**: 251.

7 Nonogaki S, Ueno T, Ito T. *Microlithography Fundamentals in Semiconductor Devices and Fabrication Technology*; 1998; Marcel Dekker, New York.

8 Vlasov YA, Bo X-Z, Sturm JCNorris DJ. *Nature* 2001; **414**: 289.

9 Colvin VL. *MRS Bulletin* 2001; **26**: 637.

10 Edrington AC, Urbas AM, DeRege P, Chen CX, Swager TM, Hadjichristidis N, Xenidou M, Fetters LJ, Joannopoulos JD, Fink Y, Thomas EL. *Adv. Mater.* 2001; **13**: 421.

11 Yang PD, Rizvi AH, Messer B, Chmelka BF, Whitesides GMStucky GD. *Adv. Mater.* 2001; **13**: 427.

12 Zein I, Hutmacher DW, Tan KC, Teoh SH. *Biomaterials* 2002; **23**: 1169.

13 Landers R, Hubner U, Schmelzeisen R, Mulhaupt R. *Biomaterials* 2002; **23**: 4437.

14 Vozzi G, Flaim C, Ahluwaliaa A, Bhatia S. *Biomaterials* 2003; **24**: 2533.

15 Chelnokov A, Wang K, Rowson S, Garoche P, Lourtioz JM. *Appl. Phys. Lett.* 2000; **77**: 2943.

16 Gratson GM, Xu M, Lewis JA. *Nature* 2004; **428**: 386.

17 Rao RB, Krafcik KL, Morales AM, Lewis JA. *Adv. Mater.* 2005; **17**: 289.

18 Tang MD, Golden AP, Tien J. *J. Am. Chem. Soc.* 2003; **125**: 12988.

19 Kennedy SR, Brett MJ, Toader O, John S. *Nano Letters* 2002; **2**: 59.

20 Cumpston BH, Ananthavel SP, Barlow S, Dyer DL, Ehrlich JE, Erskine LL, Heikal AA, Kuebler SM, Lee IYS, McCord-Maughon D, Qin JQ, Rockel H, Rumi M, Wu XL, Marder SR, Perry JW. *Nature* 1999; **398**: 51.

21 Noda S, Tomoda K, Yamamoto N, Chutinan A. *Science* 2000; **289**: 604.

22 Kawata S, Sun H-B, Tanaka T, Takada K. *Nature* 2001; **412**: 697.

23 Stellacci F, Bauer CA, Meyer-Friedrichsen T, Wenseleers W, Marder SR, Perry JW. *J. Am. Chem. Soc.* 2003; **125**: 328.

24 Wu PW, Cheng W, Martini IB, Dunn B, Schwartz BJ, Yablonovitch E. *Adv. Mater.* 2000; **12**: 1438.

25 Zhou WH, Kuebler SM, Braun KL, Yu TY, Cammack JK, Ober CK, Perry JW, Marder SR. *Science* 2002; **296**: 1106.

26 Deubel M, Von Freymann G, Wegener M, Pereira S, Busch K, Soukoulis CM. *Nature Mater.* 2004; **3**: 444.

27 Campbell M, Sharp DN, Harrison MT, Denning RG, Turberfield AJ. *Nature* 2000; **404**: 53.

28 Divliansky I, Mayer TS, Holliday KS, Crespi VH. *Appl. Phys. Lett.* 2003; **82**: 1667.

29 Divliansky IB, Shishido A, Khoo IC, Mayer TS, Pena D, Nishimura S, Keating

CD, Mallouk TE. *Appl. Phys. Lett.* 2001; **79**: 3392.

30 Yang S, Megens M, Aizenberg J, Wiltzius P, Chaikin PM, Russel WB. *Chem. Mater.* 2002; **14**: 2831.

31 Wang X, Xu JF, Su HM, Zeng ZH, Chen YL, Wang HZ, Pang YK, Tam WY. *Appl. Phys. Lett.* 2003; **82**: 2212.

32 Sharp DN, Turberfield AJDenning RG. *Phys. Rev. B* 2003; **68**: 205102.

33 Escuti MJCrawford GP. *Opt. Eng.* 2004; **43**: 1973.

34 Ullal CK, Maldovan M, Thomas EL, Chen G, Han Y-J, Yang S. *Appl. Phys. Lett.* 2004; **84**: 5434.

35 Yang S, Chen G, Megens M, Ullal CK, Han YJ, Rapaport R, Thomas EL, Aizenberg J. *Adv. Mater.* 2005; **17**: 435.

36 Fernandez A, Bedrossian PJ, Baker SL, Vernon SPKania DR. *IEEE Transactions on Magnetics* 1996; **32**: 4472.

37 Vogelaar L, Nijdam W, van Wolferen H, de Ridder RM, Segerink FB, Fluck E, Kuipers L, van Hulst NF. *Adv. Mater.* 2001; **13**: 1551.

38 Kang JW, Kim MJ, Kim JP, Yoo SJ, Lee JS, Kim DY, Kim JJ. *Appl. Phys. Lett.* 2003; **82**: 3823.

39 Petsas KI, Coates AB, Grynberg G. *Phys. Rev. A* 1994; **50**: 5173.

40 Yuan L, Wang GP, Huang XK. *Opt. Lett.* 2003; **28**: 1769.

41 Cai LZ, Yang XL, Liu Q, Wang YR. *Opt. Comm.* 2003; **224**: 243.

42 Cai LZ, Yang XL, Wang YR. *J. Opt. Soc. Am. A* 2002; **19**: 2238.

43 Cai LZ, Yang XL, Wang YR. *Opt. Lett.* 2002; **27**: 900.

44 Su HM, Zhong YC, Wang X, Zheng XG, Xu JF, Wang HZ. *Phys. Rev. E* 2003; **67**: 056619.

45 Ullal CK, Maldovan M, Wohlgemuth M, Thomas EL. *J. Opt. Soc. Am. A* 2003; **20**: 948.

46 Grynberg G, Lounis B, Verkerk P, Courtois JY, Salomon C. *Phys. Rev. Lett.* 1993; **70**: 2249.

47 Dufresne ER, Spalding GC, Dearing MT, Sheets SA, Grier DG. *Rev. Sci. Instr.* 2001; **72**: 1810.

48 Curtis JE, Koss BA, Grier DG. *Opt. Comm.* 2002; **207**: 169.

49 Ladavac K, Grier DG. *Opt. Exp.* 2004; **12**: 1144.

50 Moon JH, Yang SM, Pine DJ, Chang WS. *Appl. Phys. Lett.* 2004; **85**: 4184.

51 Berger V, GauthierLafaye O, Costard E. *Electron. Lett.* 1997; **33**: 425.

52 Shishido A, Diviliansky IB, Khoo IC, Mayer TS, Nishimura S, Egan GL, Mallouk TE. *Appl. Phys. Lett.* 2001; **79**: 3332.

53 Zaidi SH, Brueck SRJ. *J. Vac. Sci. Technol. B* 1993; **11**: 658.

54 Gigli G, Rinaldi R, Turco C, Visconti P, Cingolani R, Cacialli F. *Appl. Phys. Lett.* 1998; **73**: 3926.

55 Solak HH, David C, Gobrecht J, Wang L, Cerrina F. *J. Vac. Sci. Technol. B* 2002; **20**: 2844.

56 Pang L, Nakagawa W, Fainman Y. *Appl. Opt.* 2003; **42**: 5450.

57 Visconti P, Turco C, Rinaldi R, Cingolani R. *Microelec. Eng.* 2000; **53**: 391.

58 Shoji S, Kawata S. *Appl. Phys. Lett.* 2000; **76**: 2668.

59 Lin Y, Herman PR, Darmawikarta K. *Appl. Phys. Lett.* 2005; **86**: 071117.

60 Miklyaev YV, Meisel DC, Blanco A, von Freymann G, Busch K, Koch W, Enkrich C, Deubel M, Wegener M. *Appl. Phys. Lett.* 2003; **82**: 1284.

61 Toader O, Chan TYM, John S. *Phys. Rev. Lett.* 2004; **92**: 043905.

62 Maldovan M, Thomas EL. *Nature Mater.* 2004; **3**: 593.

63 Wohlgemuth M, Yufa N, Hoffman J, Thomas LE. *Macromolecules* 2001; **34**: 6083.

64 Moon JH, Small A, Yi GR, Lee SK, Chang WS, Pine DJ, Yang SM. *Syn. Metals* 2005; **148**: 99.

65 Lee KY, LaBianca N, Rishton SA, Zolgharnain S, Gelorme JD, Shaw J, Chang THP. *J.Vac. Sci.Technol. B* 1995; **13**: 3012.

66 Shaw JM, Gelorme JD, LaBianca NC, Conley WE, Holmes SJ. *IBM J. Res. Dev.* 1997; **41**: 81.

67 Rajaraman SK, Mowers WACrivello JV. *J. Polym. Sci. A-Polym. Chem.* 1999; **37**: 4007.

68 Boey F, Rath SK, Ng AK, Abadie MJM. *J. Appl. Polym. Sci.* 2002; **86**: 518.

69 Bi YB, Neckers DC. *Macromolecules* 1994; **27**: 3683.

70 Hua YJ, Crivello JV. *Macromolecules* 2001; **34**: 2488.

71 Crivello JV, Lam JHW. *J. Polym. Sci: Polym. Chem. Ed.* 1978; **16**: 2441.

72 Crivello JV, Sangermano M. *J. Polym. Sci. A-Polym. Chem.* 2001; **39**: 343.

73 Hinsberg W, Houle FA, Sanchez M, Morrison M, Wallraff G, Larson C, Hoffnagle J, Brock P, Breyta G In *Advances in Resist Technology and Processing XVII*; Houlihan, FM, Ed.; The International Society for Optical Engineering: California, 2000; Vol. Proc. SPIE Vol. 3999, p 148.

74 Thompson LF, Willson CG, Bowden MJ. *Introduction to microlithography*, 2 nd ed.; 1994; American Chemical Society, Washington, DC.

75 Saravanamuttu K, Blanford CF, Sharp DN, Dedman ER, Turberfield AJ, Denning RG. *Chem. Mater.* 2003; **15**: 2301.

76 Beebe DJ, Moore JS, Bauer JM, Yu Q, Liu RH, Devadoss CJo BH. *Nature* 2000; **404**: 588.

77 Lee YJBraun PV. *Adv. Mater.* 2003; **15**: 563.

78 Hoffman AS. *Adv. Drug Del. Rev.* 2002; **54**: 3.

79 Yang S, Ford J, Ruengruglikit C, Huang Q, Aizenberg J. *J. Mater. Chem.* 2005; in press.

80 Yoshino K, Shimoda Y, Kawagishi Y, Nakayama K, Ozaki M. *Appl. Phys. Lett.* 1999; **75**: 932.

81 Kang D, Maclennan JE, Clark NA, Zakhidov AA, Baughman RH. *Phys. Rev. Lett.* 2001; **86**: 4052.

82 Mach P, Wiltzius P, Megens M, Weitz DA, Lin KH, Lubensky TC, Yodh AG. *Phys. Rev. E* 2002; **65**: 031720.

83 Bunning TJ, Natarajan LV, Tondiglia VP, Sutherland RL. *Ann. Rev. Mater. Sci.* 2000; **30**: 83.

84 Sutherland RL, Tondiglia VP, Natarajan LV, Bunning TJ. *Appl. Phys. Lett.* 2001; **79**: 1420.

85 Kawatsuki N, Hasegawa T, Ono H, Tamoto T. *Adv. Mater.* 2003; **15**: 991.

86 Escuti MJ, Qi J, Crawford GP. *Appl. Phys. Lett.* 2003; **83**: 1331.

87 Escuti MJ, Qi J, Crawford GP. *Opt. Lett.* 2003; **28**: 522.

88 Escuti MJ, Crawford GP. *Mol. Cryst. Liq. Cryst.* 2004; **421**: 23.

89 Tondiglia VP, Natarajan LV, Sutherland RL, Tomlin D, Bunning TJ. *Adv. Mater.* 2002; **14**: 187.

90 Robbie K, Brett MJ. *J. Vac. Sci. Technol. A* 1997; **15**: 1460.

91 Robbie K, Sit JC, Brett MJ. *J. Vac. Sci. Technol. B* 1998; **16**: 1115.